ADVANCED THEORY AND SIMULATIONS
www.advtheorysimul.com

High-Throughput Screening of Metal Organic Frameworks as Fillers in Mixed Matrix Membranes for Flue Gas Separation

*Hilal Daglar and Seda Keskin**

High-throughput computational screening of metal organic frameworks (MOFs) is performed to evaluate their performances as fillers in mixed matrix membranes (MMMs). Grand canonical Monte Carlo and molecular dynamics simulations are performed to calculate CO_2 and N_2 permeabilities of 7822 synthesized MOFs. This data are then combined with the experimentally reported gas permeability data of 14 different polymers using a theoretical permeation model. As a result, CO_2 permeabilities and CO_2/N_2 selectivities of 109 508 different types of MOF-based MMMs are estimated. The maximum CO_2/N_2 selectivity and CO_2 permeability of MOF/polymer MMMs are computed as 64.3 and 36 103 Barrer, respectively. The top 50 MOFs that significantly improve CO_2/N_2 separation performances of highly permeable polymers are identified and their potentials for separation of binary CO_2/N_2 mixture are examined at practical operating conditions. Results show that several MOFs offer significant improvements both in the gas permeability and selectivity of polymers when used as fillers in MMMs for flue gas separation. The MOF structure–membrane performance relations are also investigated for MOF/polymer MMMs, and results show that MOFs with narrow pore sizes (3.75–5.12 Å), low surface areas (<1000 $m^2\ g^{-1}$), and moderate porosities (0.41–0.58) lead to highly selective MMMs.

1. Introduction

Membrane-based CO_2 separation from flue gas, a gas mixture mainly consisting of CO_2 and N_2, has been proved to be a potential alternative to the traditional separation methods due to the cost and energy-efficient nature of the membranes in addition to their environmentally benign and versatile characteristics.[1] Polymeric membranes have been widely used for CO_2/N_2 separation and extensively reviewed in the literature[2–4] in addition to the discussion of strategies that can improve the construction of more efficient polymeric membranes.[5] Polymeric membranes offer good thermal and mechanical properties for an effective gas separation process even at elevated temperatures but the well-known trade-off between the gas permeability and selectivity of the polymeric membranes has directed the researchers to develop new membrane materials. Polymers having high gas permeabilities generally suffer from low selectivity and polymers offering high selectivity have limited gas permeabilities requiring high surface area membranes that increase the capital cost of the membrane-based separation process.[6] Mixed matrix membranes (MMMs) combine the processability and mechanical strength of polymers with the good gas separation properties of porous fillers. MMMs are hybrid membranes where the porous fillers are incorporated into the polymer matrix to enhance the permeability and selectivity of the pristine polymer. Early works focusing on zeolite-based MMMs had some practical problems due to incompatibility between polymer and zeolite, but this area has been revitalized by the discovery of new porous materials, metal organic frameworks (MOFs).[7]

MOFs are new-generation porous materials composed of metal clusters or ions connected by organic ligands to create highly porous frameworks. Due to the large diversity of available metals and ligands, many MOFs with unique physical and chemical properties have been synthesized and reported to date. Large surface areas, high pore volumes, good thermal and mechanical properties, tunable pore sizes, and functionalities of MOFs make them great candidates for gas separation applications.[8–10] MOFs have been recently used as filler particles in polymers to make MOF/polymer MMMs showing significantly better gas separation performances than the polymer membranes, and some MOF-based MMMs have been presented to exceed the Robeson's upper bound[6] established for polymeric membranes.[11–14] It has been reported that the presence of organic linkers in MOFs enables potentially better interaction with polymers compared to those with zeolites, reducing the non-selective defects at the MOF-polymer interface.[13] It is also important to note that incorporation of MOFs as fillers into polymers is much practical to accelerate the industrialization of MOFs compared to making

H. Daglar, Prof. S. Keskin
Department of Chemical and Biological Engineering
Koc University, Rumelifeneri Yolu
Sariyer 34450, Istanbul, Turkey
E-mail: skeskin@ku.edu.tr

The ORCID identification number(s) for the author(s) of this article can be found under https://doi.org/10.1002/adts.201900109

© 2019 The Authors. Published by WILEY-VCH Verlag GmbH & Co. KGaA, Weinheim. This is an open access article under the terms of the Creative Commons Attribution-NonCommercial License, which permits use, distribution and reproduction in any medium, provided the original work is properly cited and is not used for commercial purposes.

DOI: 10.1002/adts.201900109

pure, thin-film MOF membranes since fabrication of MOF-based MMMs can be envisioned with the minor adaptation of the currently existing membrane technology used for polymers. Although we are aware of the existence of several thousands of MOF structures in the literature, only a few different types of MOFs such as Cu-BTC, ZIF-8, MIL-53, and UiO-66 were used in MOF-based MMMs.[15] The large numbers of MOFs having different physical and chemical properties create a wide material space to be used as filler particles in the MMMs; however, it is also very challenging to select the most appropriate MOF fillers for a given polymer and experimentally fabricate/test the gas separation performances of all possible MOF-based MMMs. Computational studies that can predict the gas separation performances of MOF/polymer MMMs prior to experimental studies play a very important role in identifying the best performing MMMs for a gas separation of interest.

Experimental data on the gas permeability of MOFs is very limited due to the difficulty of these measurements. As a result, almost all the computational screening studies on MOF-based MMMs utilized molecular simulations to estimate the gas permeability of MOFs. This data is then combined with the available experimental gas permeability data of polymers using a theoretical permeation model in order to estimate the gas separation performance of MOF-based MMMs. In the early studies, gas permeabilities of only a small number of selected MOFs have been examined using molecular simulations,[16–18] and several MOF fillers have been shown to improve the gas separation performance of pristine polymers. Lately, with the establishment of computation-ready MOF databases[19,20] and with the advancement of molecular simulation techniques, high-throughput computational screening of MOFs has been done for different gas separations. High-throughput computational screening is very useful to efficiently identify the most promising MOF/polymer MMMs for target gas separations. For example, Altintas and Keskin[21] applied a multi-level, high-throughput computational screening methodology showing increasing computational expense and complexity at each level to study ≈3800 MOFs for CO_2/CH_4 separation. They identified the top eight MOF fillers from their screening approach and then estimated gas permeabilities and selectivities of MOF-based MMMs composed of these top MOFs and eight different polymers. Results showed that incorporation of MOFs significantly enhances CO_2 permeabilities of all polymers and even enhances CO_2/CH_4 selectivities of some polymers. Azar et al.[22] used a high-throughput computational screening approach to identify the best MOF fillers for H_2/N_2 separation and presented that incorporating MOFs into polymers almost doubles H_2 permeabilities and some MOFs provide slight enhancements in H_2/N_2 selectivities of polymers. Wilmer et al.[23] computationally screened a large number of real and hypothetical MOFs for CO_2/N_2 separation to predict the cost of carbon capture as a function of selectivity of MOF-based MMMs. They predicted that a large number of MMMs yields a cost of carbon capture <$50 per tonne of CO_2 removed. Yan et al.[24] recently performed high-throughput computational screening of covalent organic frameworks (COFs) for CO_2/CH_4 separation, and three well-performed COFs identified from their computational screening were examined as fillers in MMMs composed of four different polymers. Their results showed that some COFs can promote the polymers above the Robeson's upper bound.

In this work, we aimed to computationally screen the recent, synthesized MOF database to evaluate the potential of all possible MOF-based MMMs for CO_2/N_2 separation. A combination of the state-of-the-art molecular simulations, grand canonical Monte Carlo (GCMC) and molecular dynamics (MD), were used to assess the single-component CO_2 and N_2 permeabilities of 7822 MOFs, and this data was then combined with the experimentally reported gas permeability data of 14 different polymers using a theoretical permeation model to predict CO_2 and N_2 permeabilities of 109 508 different types of MOF/polymer MMMs. The impact of using MOF fillers on the gas separation performance of each polymer was evaluated in detail, and the top 50 MOF fillers that significantly improve the CO_2/N_2 separation performances of polymers by carrying them well above the upper bound were identified. Assessing gas permeabilities of MOF-based MMMs for mixtures is important for industrial separation applications but there is very limited data on the mixture permeabilities of both MOFs and polymers. In order to unlock the flue gas separation performances of MOF-based MMMs, we computed CO_2/N_2 mixture permeabilities of the top 50 MOFs by performing molecular simulations under the same conditions with the experiments that reported mixture permeabilities of polymers. Permeabilities and selectivities of MOF/polymer MMMs for separation of binary CO_2/N_2:15/85 mixture were predicted and compared with those calculated using the single-component gas data. Finally, we investigated the impact of structural properties of MOF fillers such as porosity, pore size, and accessible surface area on the CO_2/N_2 selectivity of MOF-based MMMs to provide insights into the proper selection of MOF fillers. These results will be useful to accelerate the design and development of new MOF-based MMMs for high-performance flue gas separation.

2. Computational Details

We used the updated version (December 2017) of the non-disordered MOF subset of the Cambridge Structural Database (CSD)[20] consisting of 70 589 MOFs and removed the solvent molecules from the pores of MOFs using the Phyton script[20] of the database to imitate the experimental activation procedure of MOFs. Zeo++ (version 0.3) software[25] was used to compute the largest cavity diameter (LCD), pore limiting diameter (PLD), accessible surface area (SA), and porosity of MOFs. More details about these calculations are available in our earlier studies.[26,27] We limited the MOF database to only include materials having SA > 0 $m^2\ g^{-1}$ and PLD > 3.75 Å for the permeation of CO_2 and N_2 molecules (kinetic diameters of 3.3 and 3.64 Å, respectively) through the pores of MOFs. MOFs for which self-diffusivities of gases were computed to be $<10^{-8}$ $cm^2\ s^{-1}$, the limit to accurately characterize molecular diffusion by the MD simulations were also eliminated, and as a result, 7822 different types of MOFs representing various structural properties were examined as fillers in this study.

In order to save computational time, molecular simulations of MOFs were initially performed at infinite dilution to compute gas permeabilities. The Henry's constants (K^0) and self-diffusivities (D^0) of CO_2 and N_2 molecules were computed at infinite dilution where the adsorbate–adsorbate interactions were neglected, and 30 gas molecules were inserted into each MOF. These

© 2019 The Authors. Published by WILEY-VCH Verlag GmbH & Co. KGaA, Weinheim

simulations were performed using the RASPA simulation code.[28] The Widom particle insertion method was used to calculate K^0 values of gases at 298 K, and we set the number of initialization and production cycles to 5000 and 10 000, respectively.[29] D^0 values were calculated using the slope of the mean square displacement of the gas molecules with respect to time obtained from the MD simulations. These simulations were performed at NVT ensemble using the Nosé–Hoover thermostat[29] and 10^6 cycles with a time step of 1 fs were used. The intermolecular interactions between gas molecules and MOF atoms were defined using the Lennard–Jones (LJ) potential.

CO_2 was modeled as a three-site rigid molecule with LJ 12–6 potential, and its partial point charges were positioned at the center of each site.[30] N_2 was also represented as a three-site molecule; two sites were positioned at the N atoms and the third site was at the center of the mass with partial point charges.[31] We employed the universal force field (UFF)[32] to describe the potential parameters of MOF atoms. Since CO_2 and N_2 molecules have quadrupole moments, electrostatic interactions between the gases and framework atoms were taken into account by assigning the partial point charges to the framework atoms using the charge equilibration method (QEq)[33] existing in the RASPA. The Ewald summation was employed to calculate the electrostatic interactions.[34] The good agreement between simulations and experiments for the adsorption and diffusion of CO_2 and N_2 in many MOFs was shown in our earlier studies,[35–37] which validates the appropriateness of the force field and charge assignment method used in molecular simulations. In addition to this, we compared our simulation results with the experimentally reported single-component and mixture permeabilities of CO_2 and N_2 for several MOF membranes in our previous work.[27]

Using the results of molecular simulations, gas permeabilities of MOFs at infinite dilution (P_i^{MOF}) were computed as follows where i represents gas species:

$$P_i^{MOF} = K_i^0 \times D_i^0 \tag{1}$$

Selectivities of MOFs (S_{CO_2/N_2}^{MOF}) were computed using the ratio of permeabilities of gas species as follows:

$$S_{CO_2/N_2}^{MOF} = P_{CO_2}^{MOF} / P_{N_2}^{MOF} \tag{2}$$

We studied 14 different polymers, Matrimid,[38] Ultem,[39] polyurethane (PU),[40] poly(ether-*b*-amide) (Pebax),[41] polymethylpentene (PMP),[42] poly(bis(2-(2-methoxyethoxy)ethoxy)phosphazene)(MEEP),[43] 6FDA-2,2-bis(3,4-carboxyphenyl) hexafluoropropanedianhydride-diaminomesitylene (DAM) (6FDA-DAM),[44] 6FDA-2,3,5,6-tetramethyl-1,4-phenylenediamine (6FDA-durene),[45] polymers of intrinsic microporosity-7 (PIM-7),[46] poly(dimethylsiloxane) (PDMS),[47] modified poly(dimethylsiloxane) (modified PDMS),[48] polymers of intrinsic microporosity-1 (PIM-1),[49] poly(trimethylgermylpropyne) (PTMGP),[50] and poly(trimethylsilypropyne) (PTMSP)[50] in this work. Among these polymers, Matrimid, Ultem, PU, Pebax, PMP, PDMS, 6FDA-DAM, and 6FDA-durene were studied since they are commonly used in the experimental studies. Additionally, we examined MEEP, PIM-1, PIM-7, modified PDMS, PTMGP, and PTMSP since these polymers are close to the Robeson's upper bound established for CO_2/N_2 separation.[6] Single-component CO_2 and N_2 permeabilities of these polymers are collected from the literature and given in Table S1, Supporting Information.

In a previous study, Erucar and Keskin[17] showed that predictions of the modified Felske model has the best agreement with the experiments reporting the CO_2 permeabilities of IRMOF-1/Matrimid MMMs among the theoretical permeation models that consider non-ideal interfacial morphology. Motivated from these results, we used the modified Felske model in this study to estimate the separation performance of all possible MOF-based MMMs for which experimental gas permeability data are not currently available. The modified Felske model predicts the gas permeabilities of MMMs (P^{MMM}) based on the gas permeability of polymer (P^P), permeability of MOF (P^{MOF}), volume fraction of MOF filler (ϕ) within the polymer matrix, and several constants accounting for the interfacial morphology as follows:

$$P^{MMM} = P^P \times \left[\frac{1 + 2 \times [(\beta - \gamma) / (\beta + 2\gamma)] \times \phi}{1 - [(\beta - \gamma) / (\beta + 2\gamma)] \times \phi \times \varphi}\right] \tag{3}$$

$$\beta = (2 + \delta^3) \times \lambda_{mp} - 2 \times (1 - \delta^3) \times \lambda_{1p}$$

$$\gamma = (1 + 2 \times \delta^3) - (1 - \delta^3) \times \lambda_{ml} \tag{4}$$

$$\varphi = 1 + \left[\frac{(1 - \varphi_m)}{(\phi_m)^2}\right] \times \phi$$

In this model, λ_{mp} is the permeability ratio of P^{MOF}/P^P, λ_{lp} is the permeability ratio of P^I/P^P, P^I is the permeability of interphase, P^P/β^* where the value of β^* was taken as 3 following the literature,[51,52] λ_{ml} is the permeability ratio of P^{MOF}/P^I, δ is the ratio of outer radius of the interfacial shell. Parameters used in Equation (4), δ and ϕ_m, were taken as 1.18 (obtained for Matrimid/carbon molecular MMM system[53]) and 0.64 (representing the maximum packing volume fraction of the fillers[54]), respectively. Furthermore, we also showed that gas permeability predictions of the modified Felske model are in good agreement with the experimentally measured CO_2 and N_2 permeability data for various MOF-based MMMs composed of different MOFs and polymers as we will discuss below. The volume fraction of MOF fillers in MMMs was used as 0.3 throughout this work following the experimentally fabricated MOF-based MMMs. More details about the usage of this permeation model are available in our previous works.[16,17] Once the gas permeability of MOF filler computed at infinite dilution as explained above, P^{MOF}, experimentally reported gas permeability of polymer collected from the literature, P^P, and the volume fraction of MOF filler, ϕ, were inserted into Equation (3), gas permeability of MMM (P^{MMM}) was calculated. Selectivity of a MOF-based MMM (S_{CO_2/N_2}^{MMM}) was calculated as the ratio of gas permeabilities as follows:

$$S_{CO_2/N_2}^{MMM} = P_{CO_2}^{MMM} / P_{N_2}^{MMM} \tag{5}$$

After we estimated gas permeabilities of all MOF-based MMMs at infinite dilution, we aimed to examine mixture separation performance of MOF-based MMMs. We identified the top 50 MOF fillers for highly permeable polymers which lead to the MMMs having the highest CO_2 selectivities. We searched for the available CO_2/N_2 mixture gas permeability data of polymers

© 2019 The Authors. Published by WILEY-VCH Verlag GmbH & Co. KGaA, Weinheim

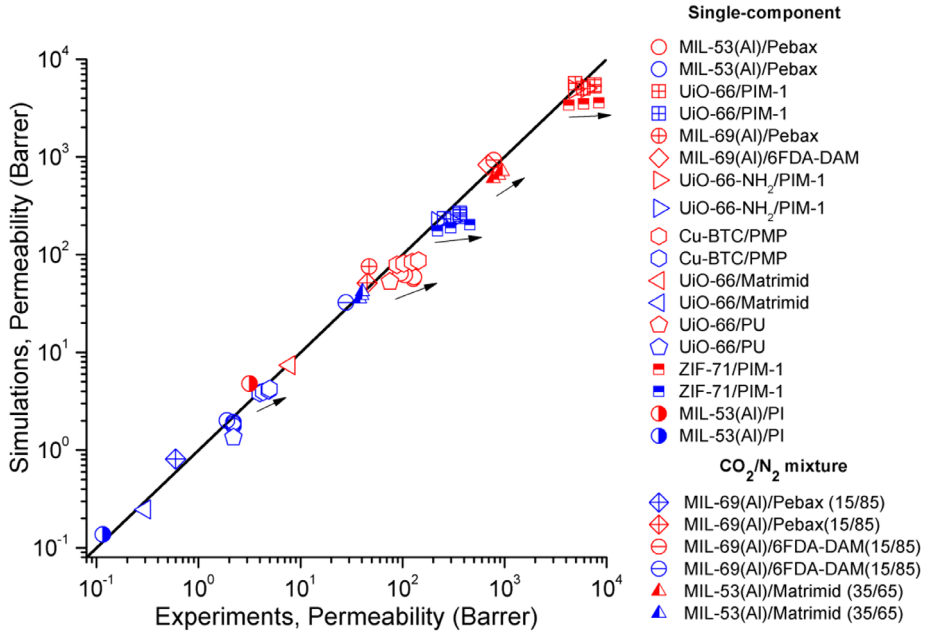

Figure 1. Comparison of experimental and simulated gas permeabilities of MOF-based MMMs. Red (blue) color represents CO_2 (N_2) permeabilities of MMMs. Arrows represent increase of MOF loading in the MMM. Details of the experimental permeability measurements are given in Table S3, Supporting Information.

and obtained this data for four polymers, Pebax, 6FDA-DAM, Matrimid, and PIM-1, as reported in Table S2, Supporting Information. In order to predict the CO_2/N_2 mixture permeabilities of MOF-based MMMs composed of these polymers, we performed GCMC and MD simulations for the top 50 MOF fillers considering the same gas compositions under the same measurement conditions of these polymers as given in Table S2, Supporting Information. In binary mixture adsorption and diffusion simulations, gas–gas and gas–MOF interactions were all considered. The same potentials and force fields as described above were used in GCMC and MD simulations. Intermolecular interactions were truncated at a cut-off distance of 13 Å and the simulation cell lengths in each dimension were increased to at least 26 Å. In molecular simulations, 5000 cycles for initialization and 10 000 cycles for ensemble averages were used. After GCMC simulations, 10^6 cycles were used in the NVT ensemble using a time step of 1 fs in MD simulations and details of these simulations are available in the literature.[29,55] Mixture permeabilities of MOF fillers were computed using,

$$P_i^{\text{MOF, mix}} = c_i^{\text{mix}} \times D_i^{\text{mix}} / f_i \tag{6}$$

where c_i, D_i, and f_i correspond to the adsorbed gas loading of species i computed from GCMC simulations, self-diffusion coefficient of gas species i computed from MD simulations, and feed side partial pressure of the gas species i, respectively. Selectivities of MOF fillers at the binary mixture conditions were computed as the ratio of gas permeabilities as follows:

$$S_{CO_2/N_2}^{\text{MOF, mix}} = P_{CO_2}^{\text{MOF, mix}} / P_{N_2}^{\text{MOF, mix}} \tag{7}$$

Once the mixture gas permeability of MOF filler, $P_i^{\text{MOF, mix}}$, experimentally reported gas permeability of polymer collected from the literature, $P^{P,\text{mix}}$, and the volume fraction of MOF filler, ϕ, were inserted into Equation (3), mixture gas permeability of MMM ($P^{\text{MMM, mix}}$) was calculated. Mixture selectivity of a MOF-based MMM ($S_{CO_2/N_2}^{\text{MMM, mix}}$) was calculated as the ratio of mixture permeabilities as follows:

$$S_{CO_2/N_2}^{\text{MMM, mix}} = P_{CO_2}^{\text{MMM, mix}} / P_{N_2}^{\text{MMM, mix}} \tag{8}$$

3. Results and Discussions

We first compared simulated gas permeability of MOF-based MMMs with the experimental gas permeability data available in the literature. In order to be consistent with the experimental conditions, we carried out our molecular simulations under the same pressure and temperature, using the same gas composition and membrane thickness reported in the experiments. Details of these conditions are given in Table S3, Supporting Information. **Figure 1** shows the good agreement between experimentally measured and simulated single-component CO_2 and N_2 permeabilities for ten different MOF-based MMMs and CO_2/N_2 mixture permeabilities of three different MOF-based MMMs. Simulations generally underestimate the experimentally reported gas permeabilities, especially as the weight percent of MOF fillers in the MMMs increases. Experimentally fabricated MMMs may have defects which may act as non-selective regions resulting in high gas permeabilities. Furthermore, the increase of the filler loading in the polymer matrix may cause agglomeration of the MOF particles in some regions of the polymer, which results in high gas permeabilities for the experimentally fabricated MOF-based MMMs. Our calculations are based on a theoretical model that considers the non-ideal morphology of MMM; however, mathematical permeation models are generally

© 2019 The Authors. Published by WILEY-VCH Verlag GmbH & Co. KGaA, Weinheim

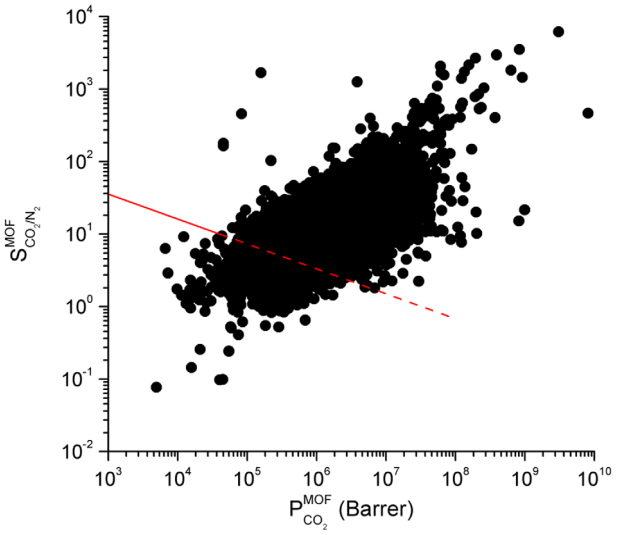

Figure 2. Simulated CO_2/N_2 selectivity and CO_2 permeability of MOFs computed at infinite dilution at 298 K. Red line represents the Robeson's upper bound for membrane-based CO_2/N_2 separation.

limited in terms of representing the distribution and agglomeration of the filler particles in polymers, especially at high filler loadings.

As shown in Figure 1, only a variety of MOFs (MIL-53(Al), UiO-66, UiO-66-NH_2, Cu-BTC, ZIF-71, MIL-69(Al)), and polymers (Pebax, PIM-1, 6FDA-DAM, PMP, Matrimid, PU, PI) has been used to fabricate MOF-based MMMs to date. Therefore, we have limited data on the CO_2/N_2 separation performances of MOF-based MMMs. Considering the existence of high numbers of synthesized MOFs and polymers, a large diversity of MMMs which may offer higher CO_2/N_2 selectivities and higher CO_2 permeabilities can exist. Motivated from the good agreement between experiments and simulations for the CO_2/N_2 separation performances of MOF-based MMMs as shown in Figure 1, we aimed to predict CO_2 permeabilities and CO_2/N_2 selectivities of all possible MOF/polymer MMMs for which experimental gas permeability data is not currently available. In order to predict the gas permeability of MOF-based MMMs, permeabilities of MOFs are required as described in Equation (3). We used molecular simulations to compute CO_2 and N_2 permeabilities of 7822 MOFs at infinite dilution to save significant computation time and showed the results in **Figure 2** together with the Robeson's upper bound. The CO_2 permeabilities of MOFs were computed to range from 4.94×10^3 to 8.13×10^9 Barrer, whereas their CO_2/N_2 selectivities were calculated to be between 7.68×10^{-2} and 6167. The red line represents the Robeson's upper bound[6] established for the CO_2/N_2 separation performances of polymers. Experimental CO_2 permeabilities of polymers were reported to be between 5 and 7×10^4 Barrer, and CO_2/N_2 selectivities were reported to be between 8 and 220. Since MOFs generally have higher CO_2 permeabilities than the polymers, we extended the upper bound using dashed lines in Figure 2. These results suggest that MOFs can be promising filler particles to be used in MMM applications to enhance both the CO_2 permeabilities and CO_2/N_2 selectivities of polymers.

Using the simulation results of 7822 MOFs and experimentally reported data of 14 polymers, we predicted the CO_2 permeability and CO_2/N_2 selectivities of 109 508 different MOF-based MMMs as shown in **Figure 3**a. We highlight that this is the largest number of MOF-based MMMs for which synthesized, real MOFs were considered as fillers using high-throughput molecular simulations. Figure 3a shows that using MOFs as fillers in polymers having CO_2 permeabilities ≤250 Barrer, (Matrimid, Ultem, PU, Pebax, PMP, and MEEP) improves the CO_2 permeabilities of these polymers without significantly changing their CO_2/N_2 selectivities. For example, every MOF can increase the CO_2 permeability of Matrimid from 8.5 to 10.6 Barrer without changing its CO_2 selectivity. Regardless of the identity of the MOF incorporated into Matrimid, all MOF/Matrimid MMMs are located under the upper bound. In other words, none of the MOFs we examined in this work was able to carry Matrimid, Ultem, PU, Pebax, or PMP above the upper bound due to the very low CO_2 permeabilities of polymers.

6FDA-DAM, 6FDA-durene, PIM-7, and modified PDMS represent the polymers having CO_2 permeabilities between 550 and 2050 Barrers. The CO_2 permeabilities of these polymers increase upon the incorporation of MOF fillers while CO_2/N_2 selectivities of MOF-based MMMs become either higher or lower than those of pristine polymers. For instance, the CO_2 permeability of PIM-7 is 1100 Barrer, while the CO_2 permeabilities of MOF/PIM-7 MMMs range from 1200 to 1369 Barrer, showing the permeability improvement upon the incorporation of MOF fillers into the polymer. The CO_2/N_2 selectivity of PIM-7 membrane is 26.2, whereas selectivities of MOF/PIM-7 MMMs were computed to be in the range of 23–32.5, indicating that some MOF fillers enhance the selectivity of PIM-7 whereas some other MOFs may decrease it. Finally, we examined the effect of using MOF fillers in the polymers having already high CO_2 permeabilities, >3000 Barrer, such as PDMS, PTMSP, PIM-1, and PTMGP. Figure 3a shows that the identity of the MOF is very important for these polymers because MOFs can increase or decrease both CO_2 permeabilities and CO_2/N_2 selectivities. For example, PTMSP has the highest CO_2 permeability, 29 000 Barrer, among the 14 polymers we studied. The CO_2 permeabilities of MOF/PTMSP MMMs were computed to be 20 294–36 102 Barrers, showing that some MOF fillers improve the CO_2 permeability whereas some others decrease it. The CO_2/N_2 selectivity of MOF/PTMSP MMMs was calculated to be between 6.2 and 18.3, whereas selectivity of the pure polymer was 10.7. This example shows the importance of the appropriate selection of MOF for the polymers offering high permeability but suffering from low selectivity.

The most important feature of Figure 3a is that PIM-1, PTMSP, and PTMGP are the polymers that are close to the upper bound and with the addition of some MOF fillers, MMMs of these polymers can exceed the upper bound. Therefore, we specifically focused on these three polymers in Figure 3b and identified the top 50 common MOF fillers that lead to MMMs having the highest CO_2/N_2 selectivities. Stars in Figure 3b show the top 50 MOF fillers that significantly enhance the CO_2/N_2 separation performances of PIM-1, PTMGP, and PTMSP in MMM applications and the refcodes of the top 50 MOF fillers are given in Table S4, Supporting Information. For example, CO_2 permeability and CO_2/N_2 selectivity of PIM-1 are 4700 Barrer and 19.3, respectively, locating this polymer under the upper bound. We

© 2019 The Authors. Published by WILEY-VCH Verlag GmbH & Co. KGaA, Weinheim

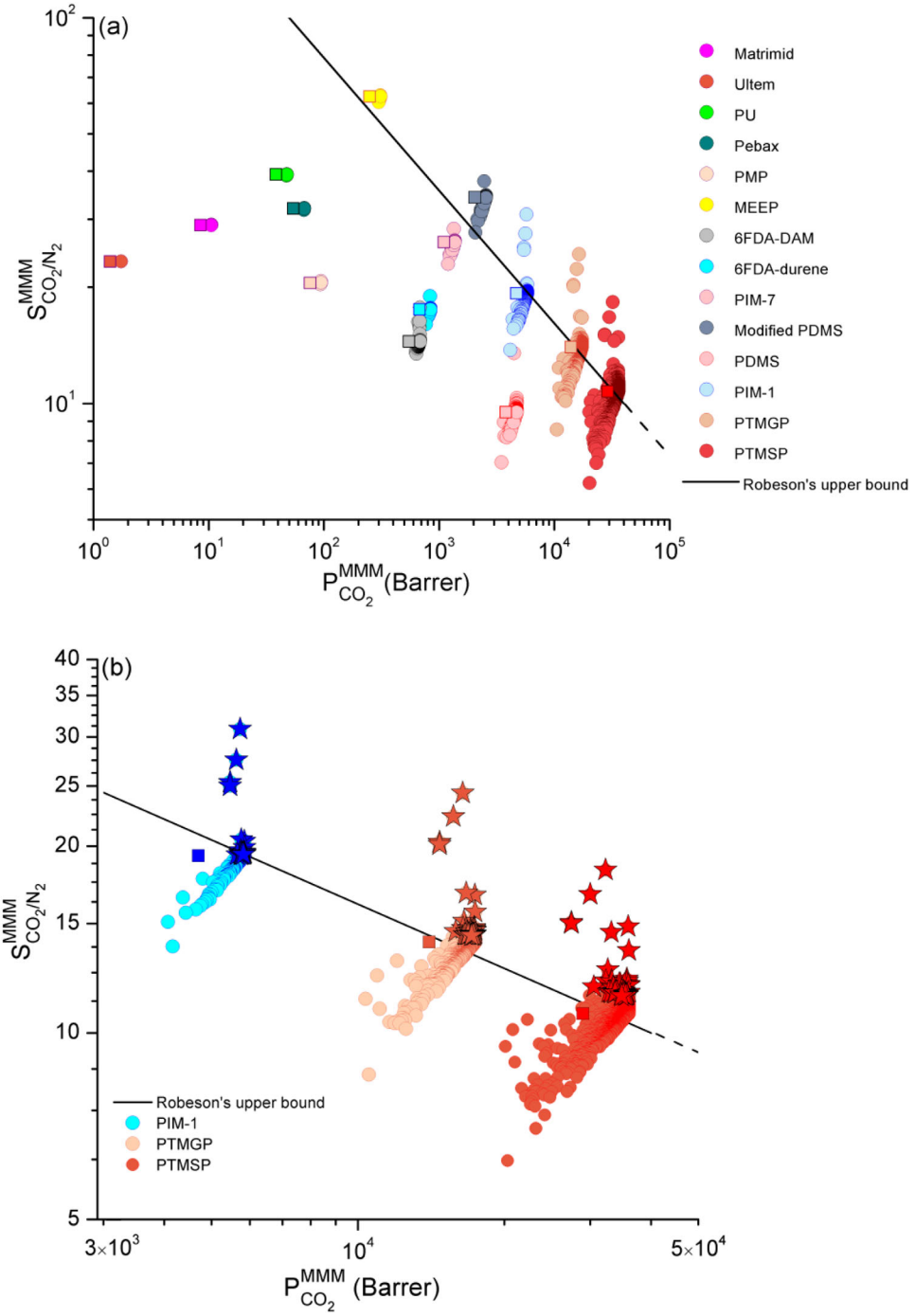

Figure 3. a) Predicted CO_2/N_2 selectivities and CO_2 permeabilities of 109 508 MOF-based MMMs. The squares (circles) represent pure polymers (MOF-based MMMs). b) Predicted CO_2/N_2 selectivities and CO_2 permeabilities of MOF-based MMMs composed of PIM-1, PTMGP, and PTMSP. The stars represent the top 50 MOF fillers providing the highest CO_2/N_2 selectivity for MMMs.

predicted the CO_2 permeabilities and CO_2/N_2 selectivities of MOF/PIM-1 MMMs composed of the best 50 MOF fillers in the range of 5462–5848 Barrers and 19.4–31, respectively. Due to the enhanced CO_2 permeabilities and selectivities, MOF/PIM-1 MMMs exceed the upper bound. Similarly, the same 50 MOF fillers enhanced the CO_2 permeability of PTMGP from 14 000 Barrer to 14 711–17 402 Barrers. Except 2 MOFs, the CO_2 permeability of PTMSP also increased from 29 000 Barrer to a range of 30 010–35 986 Barrers. The CO_2/N_2 selectivity of PTMGP (PTMSP) also increased from 14 (10.7) to 14.3–24.4 (11.5–18.3) with the addition of the top MOF fillers. We note that MMMs composed of PTMGP and PTMSP and the top 50 MOFs all exceed the upper. It is also important to note that achievable gas permeability of an MOF-based MMM that we predicted is actually

© 2019 The Authors. Published by WILEY-VCH Verlag GmbH & Co. KGaA, Weinheim

limited by the theoretical permeation model. If the gas permeability of the MOF is significantly higher than that of the polymer, $P^{MOF} \gg P^{P}$, then the modified Felske model given in Equation (3) reduces to $P^{MMM} = P^{P} \times 1.24$ at a filler volume fraction of 0.3. That means the maximum achievable gas permeability of an MOF-based MMM is 1.24 times higher than that of the polymer.

We so far predicted CO_2/N_2 separation performances of MOF-based MMMs using the single-component gas simulation data of MOFs performed at infinite dilution and using the experimentally reported single-component gas permeability data of polymers. This approach was used because a) pure gas permeabilities of polymers are commonly measured and reported in the literature due to the complexity of multi-component mixture permeability measurements and b) performing mixture simulations for thousands of MOF fillers at a pre-defined pressure is computationally much more expensive compared to performing single-component gas simulations at infinite dilution where the adsorbate–adsorbate interactions are neglected. It would be very useful to assess the CO_2/N_2 mixture separation performances of MOF-based MMMs under practical operation conditions to unlock their real potentials for industrial applications. With this motivation, we performed molecular simulations of adsorption and diffusion of CO_2/N_2:15/85 mixtures at 1 bar, 298 K for the top 50 MOF fillers.

Figure 4a compares the CO_2/N_2 selectivities and CO_2 permeabilities of the top 50 MOFs computed at mixture conditions with those calculated at infinite dilution. MOFs generally have lower CO_2 permeabilities (4.03×10^3–6.34×10^5 Barrer) and lower N_2 permeabilities (6.9–1.41×10^4 Barrer) at the binary mixture conditions compared to CO_2 permeabilities (4.54×10^4–6.6×10^6 Barrer) and N_2 permeabilities (9.4×10^1–2.23×10^4 Barrer) computed at infinite dilution. Since the decrease in N_2 permeabilities is more pronounced than the decrease in CO_2 permeabilities, higher CO_2/N_2 selectivities (8–16 628) were generally observed at binary mixture conditions compared to the ones computed at infinite dilution (21–1679). The decrease in the gas permeabilities can be explained by the decreases in the adsorption amounts and self-diffusivities of the gas components due to the competition between CO_2 and N_2 molecules.[56] An important result of Figure 4a is that the best 50 MOFs were still above the upper bound when their permeabilities were computed using the mixture simulations. This indicates that screening the MOFs at infinite dilution condition using the single-component gas simulations is an efficient strategy to quickly identify the best MOFs for the separation of binary CO_2/N_2 mixture.

In order to estimate the CO_2/N_2 mixture separation performances of MOF/polymer MMMs, we collected available mixture permeability data of polymers from the literature. Gas permeabilities of Matrimid, Pebax, 6FDA-DAM, and PIM-1 were experimentally reported at different pressures for different gas compositions. We performed GCMC and MD simulations of MOFs under the same conditions with these experiments. Figure 4b shows the CO_2 permeabilities and CO_2/N_2 selectivities of 200 MOF-based MMMs composed of the top 50 MOF fillers and 4 polymers, Pebax, 6FDA-DAM, Matrimid, and PIM-1. This is the largest number of MOF-based MMMs for which CO_2/N_2 mixture separation performances were predicted. Results shown in Figure 4b indicate that MOF/polymer MMMs are promising for the separation of binary CO_2/N_2 mixtures with various

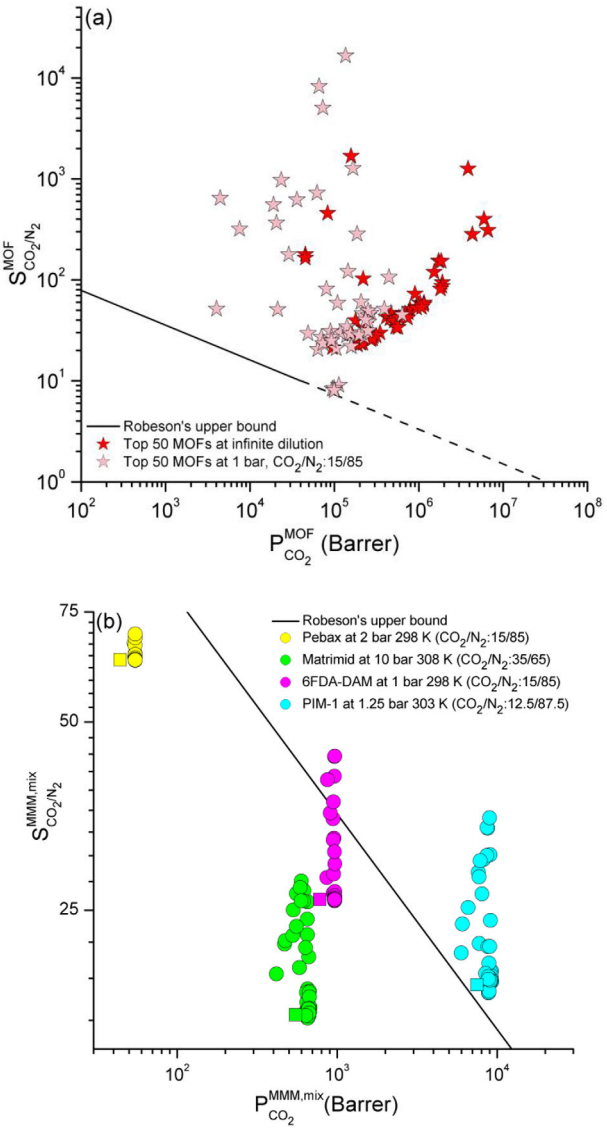

Figure 4. a) Predicted CO_2/N_2 selectivities and CO_2 permeabilities of the top 50 MOFs using single-component gas simulations performed at infinite dilution and using binary CO_2/N_2 mixture simulations performed at 1 bar, 298 K. b) Predicted CO_2/N_2 selectivities and CO_2 permeabilities of MOF-based MMMs for mixture separation. The squares (circles) represent gas permeability and selectivity of polymers (MOF-based MMMs).

compositions. For example, the CO_2 permeability and CO_2/N_2 selectivity of Pebax were reported as 44 Barrer and 63, respectively, at 2 bar, 298 K for CO_2/N_2:15/85 mixture.[44] The CO_2 permeabilities and CO_2/N_2 selectivities of MOF/Pebax MMMs were predicted as ≈54 Barrer and 63–69, respectively, showing both the permeability and selectivity improvement upon the incorporation of MOF fillers. However, these improvements were not enough to carry the Pebax above the upper bound. The CO_2 permeability and CO_2/N_2 selectivity of Matrimid were measured as 550.3 Barrer and 17, respectively, at 10 bar, 308 K for the separation of CO_2/N_2:35/65 mixture.[57] Predicted CO_2 permeabilities and CO_2/N_2 selectivities of MOF/Matrimid MMMs were in the range of 418–676 Barrers and 16.8–27.9,

© 2019 The Authors. Published by WILEY-VCH Verlag GmbH & Co. KGaA, Weinheim

Table 1. Comparison of separation performances of four polymers that have both single-component and mixture permeability measurements.

Polymer	Condition	$P^{P}_{CO_2}$ [Barrer]	$P^{P}_{N_2}$ [Barrer]	$S^{P}_{CO_2/N_2}$	$P^{MMM}_{CO_2}$ [Barrer]		$P^{MMM}_{N_2}$ [Barrer]		$S^{MMM}_{CO_2/N_2}$	
					Max.	Min.	Max.	Min.	Max.	Min.
Pebax	SG 10 bar, 308 K	54.4	1.7	32.0	67.7	67.7	2.1	2.1	32.4	32.0
Pebax	GM (15/85) 2 bar, 298 K	44.0	0.7	62.9	54.8	54.4	0.9	0.8	69.2	62.8
Matrimid	SG isochoric, 295 K	8.5	0.2	29.0	10.6	10.6	0.3	0.3	29.1	29.0
Matrimid	GM (35/65) 10 bar, 308 K	550.3	32.4	17.0	676.1	417.5	39.4	30.0	27.9	16.8
6FDA-DAM	SG 1 bar, 298 K	550	38	14.5	684.7	678.6	47.3	38.5	17.7	14.5
6FDA-DAM	GM (15/85) 1 bar, 298 K	780.0	30.0	26.0	970.2	863.2	37.3	21.5	44.1	25.9
PIM-1	SG isochoric, 313 K	4700.0	243.0	19.3	5849.4	5462.1	300.7	185.4	30.9	19.4
PIM-1	GM (12.5/87.5) 1.25 bar, 303 K	7500.0	395.0	19.0	9256.4	5975.7	481.9	255.1	35.2	18.4

SG, single-component gas; GM, gas mixture.

respectively, but these improvements were not enough to locate the Matrimid-based MMMs above the upper bound. The CO_2 permeability and CO_2/N_2 selectivity of 6FDA-DAM were reported as 780 Barrer and 26, respectively, at 1 bar, 298 K for separation of CO_2/N_2:15/85 mixture.[58] We predicted CO_2 permeabilities of MOF/6FDA-DAM MMMs in the range of 863–970 Barrer and CO_2/N_2 selectivities as 26–44 under the same operating conditions. These results showed the positive effect of using MOF fillers on the CO_2/N_2 mixture separation performance of 6FDA-DAM. Figure 4b also shows that four MOFs could carry 6FDA-DAM membrane above the Robeson's upper bound. The CO_2 permeability and CO_2/N_2 selectivity of PIM-1 were reported as 7500 Barrer and 19, respectively, at 1.25 bar, 303 K for the separation of CO_2/N_2:12.5/87.5 mixture.[59] We predicted CO_2 permeabilities and CO_2/N_2 selectivities of MOF/PIM-1 MMMs as 5976–9256 Barrer and 18.4–35.2, respectively. Some MOFs were found to increase the CO_2 permeability of PIM-1 at the expense of a slight decrease in its selectivity and all MOF/PIM-1 membranes were located above the upper bound.

For the four polymers that we studied in Figure 4b, single-component gas permeability data also exist in the literature and we compared the predicted gas permeabilities of MOF-based MMMs composed of these polymers at single-component and mixture cases. Although operating pressure, temperature, and composition of the gas mixtures are different for the polymeric membranes, **Table 1** shows that the CO_2 permeabilities and CO_2/N_2 selectivities of MOF-based MMMs that we computed at mixture conditions are generally higher than the ones computed at single-component gas condition. For example, for MOF/6FDA-DAM MMMs, the maximum CO_2 permeability and CO_2/N_2 selectivity were predicted as 684.7 Barrer and 17.7 at single-component gas conditions at 1 bar, 298 K. The maximum value of CO_2 permeability and selectivity of MOF/6FDA-DAM MMMs were calculated as 970.2 Barrer and 44.1, respectively, for the separation of CO_2/N_2:15/85 mixture under the same pressure and temperature. The higher CO_2 permeability and selectivity of MMMs at mixture condition compared to the single-component gas condition can be explained by the higher CO_2 permeability and selectivity of pristine polymer. For example, Jorge and coworkers[58] reported both the single-component and mixture permeabilities of 6FDA-DAM and showed that CO_2 permeability increased from 550 to 780 Barrer when CO_2/N_2 mixture was considered, whereas N_2 permeability decreased from 38 to 30 Barrer because of the higher solubility of CO_2 in glassy polymers, resulting in higher mixture selectivity than the ideal selectivity. Similar discussion is valid for PIM-1. Single-component CO_2 and N_2 permeabilities of PIM-1 were measured as 4700 and 243 Barrers, respectively.[60] We predicted single-component CO_2 and N_2 permeabilities of MOF/PIM-1 MMMs as 5462–5849 Barrers and 185–301 Barrers, respectively with ideal CO_2/N_2 selectivities of 19.4–30.9 as shown in Figure 3a. For CO_2/N_2:12.5/87.5 mixture, CO_2 and N_2 permeability of PIM-1 were measured as 7500 and 395 Barrer, respectively.[59] Mixture CO_2 and N_2 permeabilities of MOF/PIM-1 MMMs were predicted as 5976–9256 and 255–482 Barrers, respectively. Mixture selectivity of MOF/PIM-1 MMMs was calculated to vary between 18.4 and 35.2, whereas that of PIM-1 was 19. These results show that the maximum achievable CO_2 permeability and CO_2/N_2 selectivity of MOF/PIM-1 MMMs for separation of CO_2/N_2 mixture are higher than those computed for single-component gas separation.

We finally aimed to reveal the relations between the structural properties of MOF fillers and overall gas separation performance of MOF-based MMMs. Since MOF-based MMMs composed of PIM-1 have the widest range of CO_2/N_2 selectivities, we specifically focused on this polymer to investigate the effect of structural properties of MOFs on the selectivity of MOF/PIM-1 MMMs. **Figure 5** shows the porosity of MOFs as a function of their pore sizes and accessible surface areas, and we color-coded 7822 MOFs based on CO_2/N_2 selectivities of MOF/PIM-1 MMMs computed at infinite dilution. In each figure, red symbols show MOF/PIM-1 MMMs having CO_2/N_2 selectivities (13.8–19.3) lower than the selectivity of PIM-1 (19.3). The MOFs used as fillers in these MMMs have a very wide range of LCDs (4.09–71.64 Å), PLDs (3.75–71.50 Å), porosities (0.32–0.94), and surface areas (41.84–22 299 $m^2\ g^{-1}$). Green symbols show MOF/PIM-1 MMMs having almost similar CO_2/N_2 selectivity (19.3–19.5) with that of PIM-1. These MOFs have relatively narrower LCD (PLD) ranges between 3.92–26.78 Å (3.75–25.49 Å), narrower porosities (0.28–0.86), and lower accessible surface areas (13.44–10 239 $m^2\ g^{-1}$) than the MOFs shown with red color. Blue symbols represent MOF/PIM-1 MMMs having significantly higher CO_2/N_2 selectivities (19.5–30.9) than the selectivity of pristine PIM-1. These MOFs

© 2019 The Authors. Published by WILEY-VCH Verlag GmbH & Co. KGaA, Weinheim

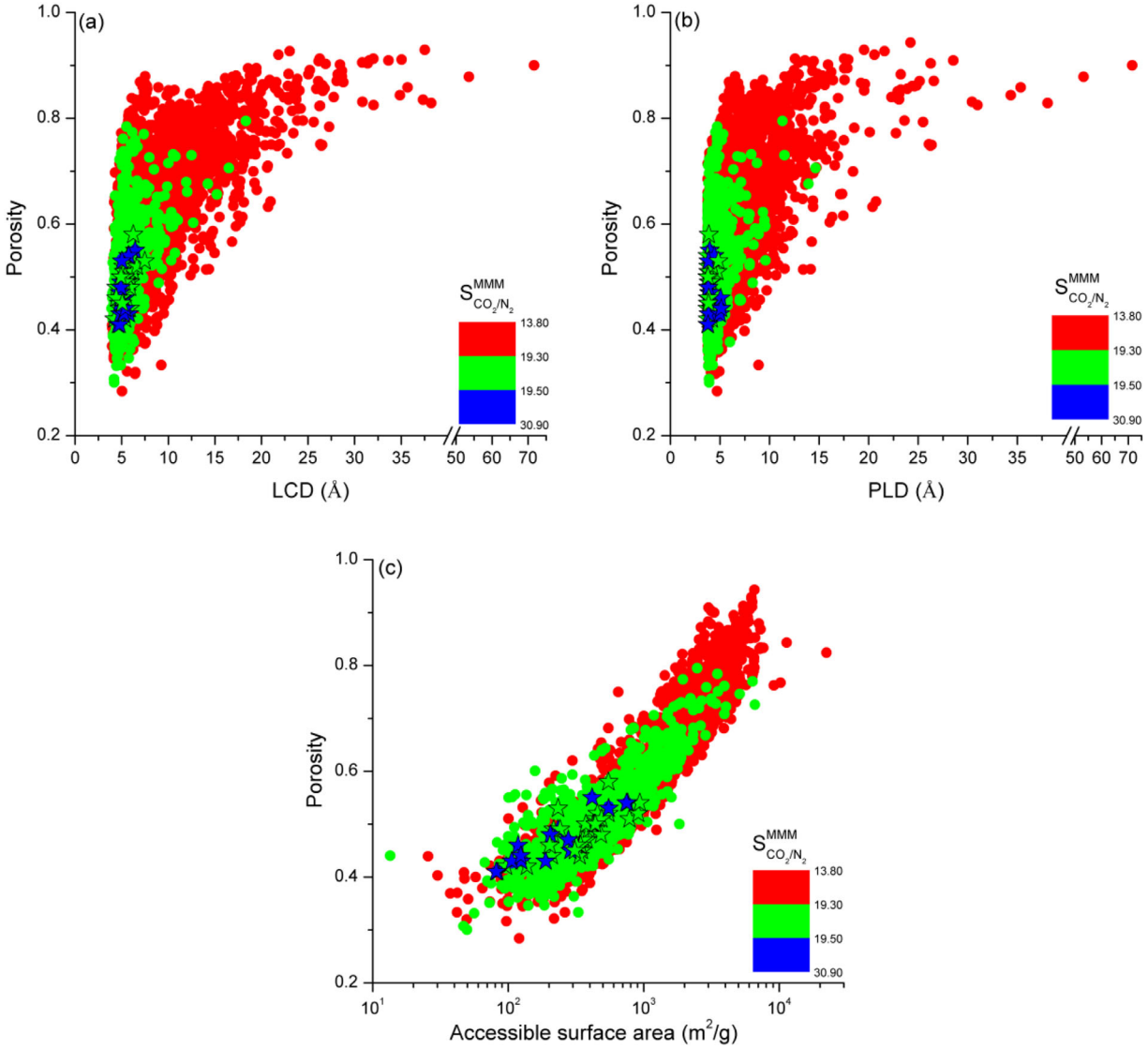

Figure 5. Porosity as a function of a) LCD, b) PLD, and c) accessible surface area of 7822 MOFs. The color scaling represents the CO_2/N_2 selectivity of MOF/PIM-1 MMMs and stars represent the MMMs composed of the top 50 MOF fillers.

have a narrow range of LCDs (4.62–7.48 Å), PLDs (3.75–5.12 Å), porosities (0.41–0.55), and surface areas (81.38–784.54 $m^2\ g^{-1}$). Figure 5a shows that as the porosity and LCD of MOFs decrease, the CO_2/N_2 selectivities of MOF/PIM-1 MMMs increase. The MMMs composed of the top 50 MOF fillers are shown with stars. The top 50 MOF fillers that offer the highest CO_2/N_2 selectivities possess porosities between 0.41 and 0.58 and LCDs between 4.2–7.5 Å. Similarly, Figure 5b shows that MOFs having narrow PLDs, 3.75–5.12 Å, with low porosities also result in highly selective MMMs. None of the MOFs having large pore sizes (LCD > 12 Å, PLD > 6 Å) leads to highly selective MMMs. Finally, Figure 5c shows that MOFs having accessible surface areas of 81.4–934 $m^2\ g^{-1}$ are the best fillers for highly selective MMMs.

At that point, we would like to note that gas separation performance of MMMs depends on several factors other than the structural properties of MOF fillers that we examined in Figure 5. For example, all our calculations predicting the gas separation performances of MOF/polymer MMMs simply assume that there is no specific compatibility problem between the MOF and the polymer such as no-adhesion between the polymer and MOF phases. In fact, the MOF/polymer interface dictates the feasibility and stability of the MMMs; therefore, a fundamental understanding of this interface is critical. Several excellent studies described the computational methods combining the density functional theory calculations and MD simulations to model MOF/polymer interfaces,[61–63] which can be used to examine the potential affinity between different MOF surfaces and polymers once the appropriate force field representing the correct description of the MMM is defined. It is also important to note that all our results are for single-component and binary mixture gas permeabilities of MOF-based MMMs and we neglected the presence of H_2O in the flue gas stream. In our recent computational work,[27] we

© 2019 The Authors. Published by WILEY-VCH Verlag GmbH & Co. KGaA, Weinheim

showed the presence of humidity can reduce both the CO_2 and N_2 permeabilities of pure MOF membranes. In an experimental study,[59] decreases in CO_2 and N_2 permeabilities of pure PIM-1 membrane were observed in the presence of water. Based on these studies, one can expect lower CO_2 and N_2 permeabilities for the MOF-based MMMs in the presence of humidity. We believe that after the best MOF candidates are computationally identified for MMM applications, it is more likely to investigate the compatibility, stability, reusability, humidity issues of membranes using experimental manners.

4. Conclusion

In this work, CO_2/N_2 separation performances of a very large number (109 508) of MOF-based MMMs composed of 7822 different types of MOFs and 14 different polymers were predicted by using high-throughput molecular simulations. Among the MOF-based MMMs that we examined, the maximum CO_2/N_2 selectivity was computed as 64.3 and the highest CO_2 permeability was estimated as 36 103 Barrers. It has been recently discussed that CO_2/N_2 selectivity greater than 50 and CO_2 permeability over 100 Barrer are required for an economic operation of CO_2 capture from flue gas.[64] There are several MOF-based MMMs which were predicted to have CO_2/N_2 selectivities and CO_2 permeabilities well beyond these desired values, highlighting the great potential of using MOFs as fillers in polymer membranes. Many MOFs can improve both the selectivity and permeability of 6FDA-DAM, 6FDA-durene, PIM-7, PDMS, modified PDMS, PIM-1, PTMGP, and PTMSP. Since highly permeable PIM-1, PTMGP, and PTMSP are very close to the upper bound, using MOFs as fillers in these polymers results in exceeding the Robeson's upper bound. We also examined binary CO_2/N_2 mixture separation performances of MOF-based MMMs and showed that MOFs have a great potential to improve the mixture selectivity of 6FDA-DAM from 26 to 44.1 and PIM-1 from 19 to 35.2. We finally showed that selecting MOF fillers with narrow pore sizes and low porosities lead to MMMs exhibiting high CO_2/N_2 selectivities.

Supporting Information

Supporting Information is available from the Wiley Online Library or from the author.

Acknowledgements

S.K. acknowledges the ERC-2017-Starting Grant. This study has received funding from the European Research Council (ERC) under the European Union's Horizon 2020 research and innovation programme (ERC-2017-Starting Grant, grant agreement No 756489-COSMOS).

Conflict of Interest

The authors declare no conflict of interest.

Keywords

flue gas separation, metal organic frameworks, mixed matrix membrane, molecular simulation

Received: June 11, 2019
Revised: July 17, 2019
Published online: August 28, 2019

[1] A. Brunetti, F. Scura, G. Barbieri, E. Drioli, *J. Membr. Sci.* **2010**, *359*, 115.
[2] S. Kim, Y. M. Lee, *Curr. Opin. Chem. Eng.* **2013**, *2*, 238.
[3] Z. Dai, L. Ansaloni, L. Deng, *Green Energy Environ.* **2016**, *1*, 102.
[4] J. Ahmad, W. U. Rehman, K. Deshmukh, S. K. Basha, B. Ahamed, K. Chidambaram, *Polym-Plast. Technol.* **2019**, *58*, 366.
[5] S. Feng, J. Ren, D. Zhao, H. Li, K. Hua, X. Li, M. Deng, *J. Energy Chem.* **2019**, *28*, 39.
[6] L. M. Robeson, *J. Membr. Sci.* **2008**, *320*, 390.
[7] M. Galizia, W. S. Chi, Z. P. Smith, T. C. Merkel, R. W. Baker, B. D. Freeman, *Macromolecules* **2017**, *50*, 7809.
[8] V. Bon, I. Senkovska, S. Kaskel, *Nanoporous Materials for Gas Storage*, Springer, Berlin **2019**.
[9] J. Yu, L.-H. Xie, J.-R. Li, Y. Ma, J. M. Seminario, P. B. Balbuena, *Chem. Rev.* **2017**, *117*, 9674.
[10] M. Ding, R. W. Flaig, H.-L. Jiang, O. M. Yaghi, *Chem. Soc. Rev.* **2019**.
[11] R. Lin, B. V. Hernandez, L. Ge, Z. Zhu, *J. Mater. Chem. A* **2018**, *6*, 293.
[12] M. Rezakazemi, A. E. Amooghin, M. M. Montazer-Rahmati, A. F. Ismail, T. Matsuura, *Prog. Polym. Sci.* **2014**, *39*, 817.
[13] B. Zornoza, C. Tellez, J. Coronas, J. Gascon, F. Kapteijn, *Microporous Mesoporous Mater.* **2013**, *166*, 67.
[14] B. Seoane, J. Coronas, I. Gascon, M. E. Benavides, O. Karvan, J. Caro, F. Kapteijn, J. Gascon, *Chem. Soc. Rev.* **2015**, *44*, 2421.
[15] E. Adatoz, A. K. Avci, S. Keskin, *Sep. Purif. Technol.* **2015**, *152*, 207.
[16] G. Yilmaz, S. Keskin, *J. Membr. Sci.* **2014**, *454*, 407.
[17] I. Erucar, S. Keskin, *Ind. Eng. Chem. Res.* **2011**, *50*, 12606.
[18] Z. Sumer, S. Keskin, *J. Nanomater.* **2016**, *2016*, 6482628.
[19] Y. G. Chung, J. Camp, M. Haranczyk, B. J. Sikora, W. Bury, V. Krungleviciute, T. Yildirim, O. K. Farha, D. S. Sholl, R. Q. Snurr, *Chem. Mater.* **2014**, *26*, 6185.
[20] P. Z. Moghadam, A. Li, S. B. Wiggin, A. Tao, A. G. Maloney, P. A. Wood, S. C. Ward, D. J. C. o. M. Fairen-Jimenez, *Chem. Mater.* **2017**, *29*, 2618.
[21] C. Altintas, S. Keskin, *ACS Sustainable Chem. Eng.* **2019**, *7*, 2739.
[22] A. Nemati Vesali Azar, S. Velioglu, S. Keskin, *ACS Sustainable Chem. Eng.* **2019**.
[23] S. Budhathoki, O. Ajayi, J. A. Steckel, C. E. Wilmer, *Energy Environ. Sci.* **2019**.
[24] T. Yan, Y. Lan, M. Tong, C. Zhong, *ACS Sustainable Chem. Eng.* **2019**, *7*, 1220.
[25] T. F. Willems, C. H. Rycroft, M. Kazi, J. C. Meza, M. Haranczyk, *Microporous Mesoporous Mater.* **2012**, *149*, 134.
[26] C. Altintas, I. Erucar, S. Keskin, *ACS Appl. Mater. Interfaces* **2018**, *10*, 3668.
[27] H. Daglar, S. Keskin, *J. Phys. Chem. C* **2018**, *122*, 17347.
[28] D. Dubbeldam, S. Calero, D. E. Ellis, R. Q. Snurr, *Mol. Simul.* **2016**, *42*, 81.
[29] D. Frenkel, B. Smit, *Understanding Molecular Simulation: From Algorithms to Applications*, Elsevier, Amsterdam **2001**.
[30] J. J. Potoff, J. I. Siepmann, *AIChE J.* **2001**, *47*, 1676.
[31] K. Makrodimitris, G. K. Papadopoulos, D. N. Theodorou, *J. Phys. Chem. B* **2001**, *105*, 777.
[32] A. K. Rappé, C. J. Casewit, K. Colwell, W. A. Goddard III, W. M. Skiff, *J. Am. Chem. Soc.* **1992**, *114*, 10024.
[33] C. E. Wilmer, R. Q. Snurr, *Chem. Eng. J.* **2011**, *171*, 775.
[34] P. P. Ewald, *Ann. Phys.* **1921**, *369*, 253.
[35] C. Altintas, G. Avci, H. Daglar, A. Nemati Vesali Azar, S. Velioglu, I. Erucar, S. Keskin, *ACS Appl. Mater. Interfaces* **2018**, *10*, 17257.

© 2019 The Authors. Published by WILEY-VCH Verlag GmbH & Co. KGaA, Weinheim

[36] Z. Sumer, S. Keskin, *Ind. Eng. Chem. Res.* **2016**, *55*, 10404.
[37] T. N. Ozturk, S. Keskin, *J. Phys. Chem. C* **2014**, *118*, 13988.
[38] S. R. Venna, M. Lartey, T. Li, A. Spore, S. Kumar, H. B. Nulwala, D. R. Luebke, N. L. Rosi, E. Albenze, *J. Mater. Chem. A* **2015**, *3*, 5014.
[39] Y. Dai, J. Johnson, O. Karvan, D. S. Sholl, W. Koros, *J. Membrane Sci.* **2012**, 401.
[40] M. A. Rodrigues, J. de Souza Ribeiro, E. de Souza Costa, J. L. de Miranda, H. C. Ferraz, *Sep. Purif. Technol.* **2018**, *192*, 491.
[41] S. Meshkat, S. Kaliaguine, D. Rodrigue, *Sep. Purif. Technol.* **2018**, *200*, 177.
[42] R. Abedini, A. Mosayebi, M. Mokhtari, *Process Saf. Environ. Prot.* **2018**, *114*, 229.
[43] C. J. Orme, M. K. Harrup, T. A. Luther, R. P. Lash, K. S. Houston, D. H. Weinkauf, F. F. Stewart, *J. Membr. Sci.* **2001**, *186*, 249.
[44] A. Sabetghadam, X. Liu, M. Benzaqui, E. Gkaniatsou, A. Orsi, M. M. Lozinska, C. Sicard, T. Johnson, N. Steunou, P. A. Wright, *Chem. - Eur. J.* **2018**, *24*, 7949.
[45] W.-H. Lin, T.-S. Chung, *J. Membrane Sci.* **2001**, 186.
[46] P. M. Budd, K. J. Msayib, C. E. Tattershall, B. S. Ghanem, K. J. Reynolds, N. B. McKeown, D. Fritsch, *J. Membrane Sci.* **2005**, *251*, 263.
[47] T. Merkel, V. Bondar, K. Nagai, B. Freeman, I. Pinnau, *J. Polym. Sci., Part B: Polym. Phys.* **2000**, *38*, 415.
[48] U. Senthilkumar, B. Reddy, *J. Membrane Sci.* **2007**, 292.
[49] G. Bengtson, S. Neumann, V. Filiz, *Membranes* **2017**, *7*, 28.
[50] T. Mizumoto, T. Masuda, T. Higashimura, *J. Polym. Sci., Part A: Polym. Chem.* **1993**, *31*, 2555.
[51] D. Q. Vu, W. J. Koros, S. Miller, *J. Membr. Sci.* **2003**, *211*, 335.
[52] T. T. Moore, R. Mahajan, D. Q. Vu, W. J. Koros, *AIChE J.* **2004**, *50*, 311.
[53] B. Shimekit, H. Mukhtar, T. Murugesan, *J. Membr. Sci.* **2011**, *373*, 152.
[54] R. Pal, *J. Colloid Interface Sci.* **2008**, *317*, 191.
[55] D. Dubbeldam, A. Torres-Knoop, K. S. Walton, *Mol. Simul.* **2013**, *39*, 1253.
[56] Z. Qiao, K. Zhang, J. Jiang, *J. Mater. Chem. A* **2016**, *4*, 2105.
[57] S. Basu, A. Cano-Odena, I. F. Vankelecom, *Sep. Purif. Technol.* **2011**, *81*, 31.
[58] M. Etxeberria-Benavides, O. David, T. Johnson, M. M. Łozińska, A. Orsi, P. A. Wright, S. Mastel, R. Hillenbrand, F. Kapteijn, J. Gascon, *J. Membr. Sci.* **2018**, *550*, 198.
[59] E. Lasseuguette, M.-C. Ferrari, S. Brandani, *Energy Procedia* **2014**, *63*, 194.
[60] A. K. Sekizkardes, V. A. Kusuma, G. Dahe, E. A. Roth, L. J. Hill, A. Marti, M. Macala, S. R. Venna, D. Hopkinson, *Chem. Commun.* **2016**, *52*, 11768.
[61] R. Semino, N. A. Ramsahye, A. Ghoufi, G. Maurin, *ACS Appl. Mater. Interfaces* **2016**, *8*, 809.
[62] M. Benzaqui, R. Semino, N. Menguy, F. Carn, T. Kundu, J.-M. Guigner, N. B. Mckeown, K. J. Msayib, M. Carta, R. Malpass-Evans, *ACS Appl. Mater. Interfaces* **2016**, *8*, 27311.
[63] R. Semino, J. Moreton, N. Ramsahye, S. Cohen, G. Maurin, *Chem. Sci.* **2018**, *9*, 315.
[64] J. Huang, J. Zou, W. W. Ho, *Ind. Eng. Chem. Res.* **2008**, *47*, 1261.

© 2019 The Authors. Published by WILEY-VCH Verlag GmbH & Co. KGaA, Weinheim